Frequency doubling in elastic mechanisms using buckling of microflexures

Farhadi Machekposhti, Davood; Herder, Just L.; Tolou, Nima

DOI
10.1063/1.5119813

Publication date
2019

Document Version
Final published version

Published in
Applied Physics Letters

Applied Physics Letters

Frequency doubling in elastic mechanisms using buckling of microflexures

Cite as: Appl. Phys. Lett. **115**, 143503 (2019); https://doi.org/10.1063/1.5119813
Submitted: 12 July 2019 . Accepted: 18 September 2019 . Published Online: 30 September 2019

Davood Farhadi Machekposhti, Just L. Herder, and Nima Tolou

Applied Physics Letters ARTICLE scitation.org/journal/apl

Frequency doubling in elastic mechanisms using buckling of microflexures

Cite as: Appl. Phys. Lett. **115**, 143503 (2019); doi: 10.1063/1.5119813
Submitted: 12 July 2019 · Accepted: 18 September 2019 ·
Published Online: 30 September 2019

Davood Farhadi Machekposhti,[a] Just L. Herder, and Nima Tolou

AFFILIATIONS

Department of Precision and Microsystem Engineering, Faculty of Mechanical, Maritime and Materials Engineering, Delft University of Technology, 2628 CD Delft, The Netherlands

[a]Author to whom correspondence should be addressed: d.farhadimachekposhti@tudelft.nl

ABSTRACT

Microtransmission mechanisms made of elastic materials present an opportunity for exploring scalable mechanical systems integrated with sophisticated functionalities. This paper shows how the fundamentally limited range of motion in elastic mechanisms can be circumvented to create a frequency doubling functionality analog to angular velocity doubling in classical gears. The proposed mechanism utilizes the elastic deformation of its internal architecture and buckling of microflexures to perform frequency doubling kinematics. We demonstrate this by the fabrication of a microtransmission device for application in mechanical wrist watches. A key benefit of the proposed method is that such a transmission system can be integrated and fabricated as an embedded part of microarchitected materials to boost the frequency characteristics of energy storage, actuators, and inertial sensors to perform adequately for different applications.

Mechanical frequency and speed multiplier transmission mechanisms are necessary for a variety of applications, including tailoring microactuators,[1–4] quantum cascade lasers,[5] mass sensing,[6] vibration energy harvesting,[7] biosensing,[8] and motion sensors and accelerometers.[9] Furthermore, integration of frequency multiplier transmission mechanisms on a local mechanical resonator can approach the limits on position and displacement measurements, which are ultimately limited by quantum mechanics.[10,11]

Classical gears are by far the most common paradigm for mechanical frequency and speed multiplication, by converting the angular velocity from an input to an output with a constant ratio. They consist of discrete components which are engaged and connected by rolling contacts and suspended by rotational hinges (revolute joints). This gives rise to numerous drawbacks and is a source of uncertainties including backlash, friction, wear, poor mechanical efficiency, and microstition.[12–14] Apart from the need for assembly and lubrication, it is difficult and it is not size and cost efficient to integrate the classical gear transmissions with the MEMS/NEMS (nano electromechanical systems)-based actuating and sensing schemes. Consequently, in vacuum (e.g., high-tech semiconductor industry and space), in biological environments (e.g., surgical instruments), or in any situation where maintenance is to be avoided, gear systems are unsuitable.

In such cases, elastic mechanisms can be used advantageously. These mechanisms move due to deformation of slender parts, thus avoiding the relative motion of rigid parts in conventional (linkage or gear) mechanisms.[15–18] As a result, friction and backlash are absent, and there is no need for lubrication or assembly. However, one key challenge is that their range of motion is severely limited: elastic elements cannot do full-cycle rotation as traditional revolute joints (e.g., ball bearings) can. As a result, to date, no solutions for precise frequency multiplication through elastic media have been reported.

In this paper, it is shown that in spite of the fundamental limitation of the motion range of elastic materials, a monolithic frequency doubler transmission is conceived, designed, and tested. The proposed methodology uses elastic deformation and internal buckling of a monolithic structure to achieve this.

The movement is based on the exchange between two instant centers of rotation enabled by the buckling in slender beams, with lengths of L_{b_1} and L_{b_2}, on two sides of the input shuttle, shown in Fig. 1(a). The buckle-sensitive beams are employed as compliant reconfigurable joints. They provide two DOF (degrees of freedom) (rotation and translation) when a tensile force is applied, undergo buckling, and relieve all planar kinematic constraints when a compressive force is applied, shown in Fig. 1(b). The rectilinear motion of the input and the output shuttles is supported via two parallel flexures with lengths of L_1, L_2, and L_3, respectively. Two double blade rotary pivots, shown in Fig. 1(c), are used to provide a relative rotation between the lever arm and both shuttles.

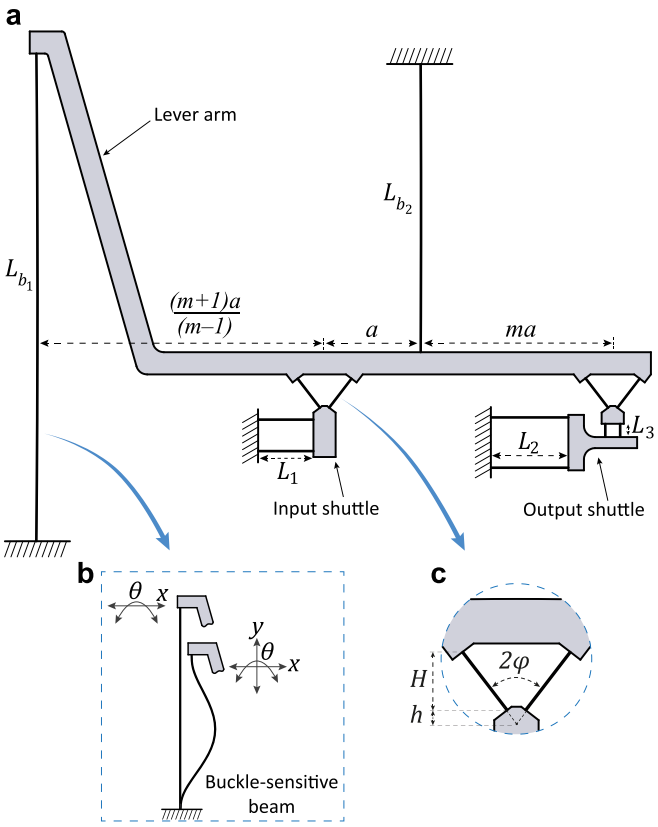

FIG. 1. (a) Schematic representation and geometric parameters of the frequency doubler transmission mechanism. (b) The buckle-sensitive beams are employed as a reconfigurable kinematic joint. (c) The geometric parameters of the double blade rotary pivot used in the design.

Input–output kinematics, the cycle of movements, and their corresponding pseudo-rigid-body kinematic models are shown in Fig. 2. As can be seen, for a forward movement of the input shuttle, the buckle-sensitive beam in the right side of the input buckles and the lever arm rotates around the virtual instant center of rotation, IC_1, which is along the left buckle-sensitive beam. This results in an forward movement of the output shuttle with a displacement of u_{out}. Likewise, the lever arm rotates around the virtual instant center of rotation, IC_2, while a backward motion is subjected to the input. As a consequence, the buckle-sensitive beam on the left side of the input shuttle undergoes buckling and results in yet another forward movement of the output, u_{out}. Since the back-and-forth movement of the input causes forward displacements for the output, the proposed monolithic structure doubles input motion frequency.

As can be seen in Fig. 1(a), the position of the buckle-sensitive beams with respect to the input and output shuttles can be chosen such that the instantaneous geometrical advantages (G.A.), m, for both cycles are equal and can be represented as

$$G.A. = \frac{u_{out}}{u_{in}} = m. \tag{1}$$

A pseudo-rigid-body model is developed to parametrize the stiffness characteristics of the proposed transmission mechanism. For given kinematics and considering a constant beam thickness over the compliant design, a symmetric actuation force-deflection profile can be established by satisfying

$$L_{b_1} = \sqrt{m+1}L_{b_2}. \tag{2}$$

The parallelogram flexures indicated with lengths L_1, L_2, and L_3, in the compliant design, are replaced by sliders and associated translational stiffness coefficients K_1, K_2, and K_3, respectively, which can be formulated as

$$K_j = \frac{24EI}{L_j^3}, \quad j = \{1, 2, 3\}, \tag{3}$$

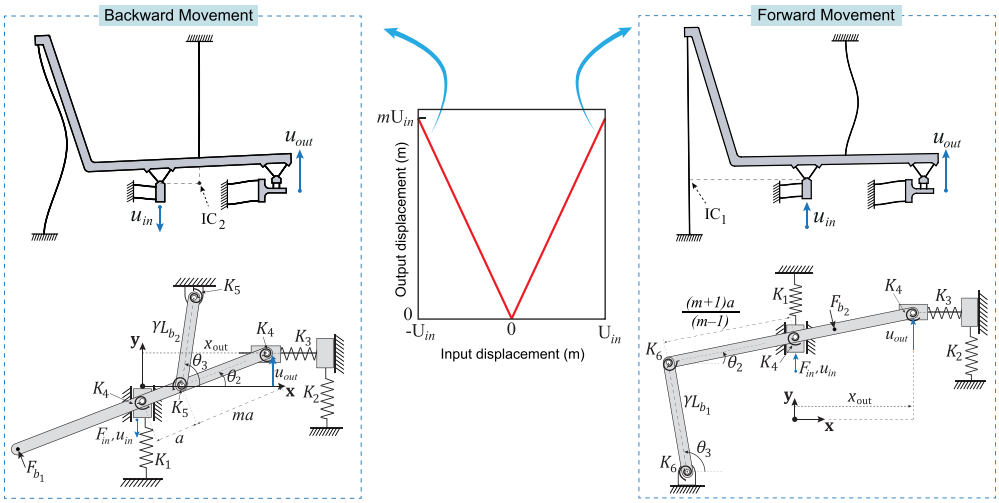

FIG. 2. Input–output displacement relationship of the proposed frequency doubler transmission mechanism (middle); cycles of movement and their corresponding pseudo-rigid-body kinematics for a backward input displacement (left) and for a forward input displacement (right).

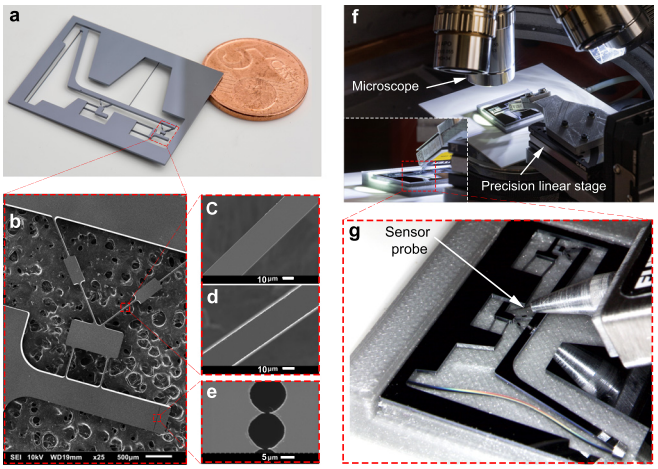

FIG. 3. (a) Fabricated microdevice on silicon using deep reactive ion etching (DRIE). (b) The scanning electron microscopy (SEM) image and zoomed-in view of the output shuttle. The SEM image of (c) top thickness of the flexures $t_1 = 18.75\,\mu$m, (d) bottom thickness of the flexures $t_2 = 24.25\,\mu$m, and (e) markers used to calibrate the optical displacement measurement, with a minimum feature size of $1.5\,\mu$m. (f) Experimental setup to evaluate the actuation force and the input–output kinematics of the microtransmission. (g) A detailed view of actuated microtransmission, corresponding to the backward movement.

where E is the Young's Modulus of the material and I is the second moment of area.

The double blade rotary pivot is modeled as a pin joint with a torsional spring K_4 located at its virtual center of rotation, where the stiffness constant is given by

$$K_4 = \frac{8EI(H^2 + Hh + h^2)\cos\varphi}{(H-h)^3}. \tag{4}$$

The buckle-sensitive beams can be considered as a fixed–fixed flexible segment when they are under tensile forces. This can kinematically be represented as a binary pseudorigid link with the length of γL_{b_1} and γL_{b_2} associated with the torsional spring K_5 at hinges. Besides, the torsional spring constant, K_5, for a fixed–fixed segment can be given by[15]

$$K_5 = 2\gamma K_\Theta \frac{EI}{L_{b_2}}, \quad K_6 = 2\gamma K_\Theta \frac{EI}{L_{b_1}}, \tag{5}$$

where $\gamma = 0.85$ is the characteristic radius factor and $K_\Theta = 2.65$ is the stiffness coefficient. In the corresponding kinematic model, the buckle-sensitive beams are replaced by their equivalent buckling forces, F_{b_2} and F_{b_1}, since they cannot pose any kinematic constraint. The buckling force can be estimated by the classical Euler–Bernoulli beam theory, and for the fixed–fixed beams, it can be expressed as

$$F_{b_j} = \frac{4\pi^2 EI}{L_{b_j}^2}, \quad j = \{1, 2\}. \tag{6}$$

Therefore, the input actuation forces, F_{in}, for both cycles can be given by applying the virtual work principle, which results in

$$\begin{aligned} F_{in} = {} & K_1 u_{in} + F_{b_2}\frac{\delta u_b}{\delta u_{in}} + K_2 u_{out}\frac{\delta u_{out}}{\delta u_{in}} + 2K_4\theta_2\frac{\delta\theta_2}{\delta u_{in}} \\ & + K_3(x_{out} - 3a)\frac{\delta x_{out}}{\delta u_{in}} + K_5\left(\theta_3 - \frac{\pi}{2}\right)\frac{\delta\theta_3}{\delta u_{in}} \\ & + K_5\left(\theta_3 - \theta_2 - \frac{\pi}{2}\right)\left(\frac{\delta\theta_3}{\delta u_{in}} - \frac{\delta\theta_2}{\delta u_{in}}\right), \end{aligned} \tag{7}$$

where $\frac{\delta(\cdot)}{\delta u_{in}}$ are kinematic coefficients and can be determined through velocity analysis.

A microdevice was dimensioned and fabricated for application in mechanical wrist watches, shown in Fig. 3(a). The device was etched on a silicon wafer with a thickness of $w = 525\,\mu$m. The design parameters, summarized in Table I, were optimized for linear input–output kinematics, with a velocity ratio of $m = 2$ and a symmetric actuation force.

A thickness of $t = 30\,\mu$m is considered for all the flexures in the design. Besides, an initial curvature with a radius of 1000 mm was implemented for both buckle-sensitive beams to ensure the buckling direction of the beams and avoid the solution convergence into higher order buckling modes in the finite element model (FEM). The designed compliant embodiment is composed of flexures with a rectangular cross section. However, the released fabricated device got a trapezoidal cross section due to the nonconstant etching rate of the deep reactive ion etching (DRIE) process. Therefore, a scanning electron microscopy (SEM) measurement was conducted to find the thickness of the flexures at the top and bottom layers, as shown in Figs. 3(c) and 3(d). The results are then applied to the FEM and the theoretical model by creating a customized cross section based on the SEM results.

A FEM model was made in ANSYS to analyze the compliant frequency doubler transmission. The beam element based on the Timoshenko beam theory (BEAM188) was used for the flexures. Moreover, orthotropic material properties for a standard (100) silicon wafer were considered to investigate the device further: $E_x = E_y = 169\,GPa$, $E_z = 130$ GPa, $\nu_{yz} = 0.36$, $\nu_{zx} = 0.28$, $\nu_{xy} = 0.064$, $G_{yz} = G_{zx} = 79.6$ GPa, $G_{xy} = 50.9$ GPa, $\rho = 2330\,\mathrm{kg/m^3}$. The FEM was evaluated, while the maximum Von Mises stress was limited by a maximum allowable stress of 200 MPa. This value is selected far below the maximum yield strength of the silicon, which is about 6 GPa. This was an industrial constraint and was considered to prevent any risk of crack growth in the silicon crystal of the microdevices.

An experimental setup was constructed to evaluate the actuation stiffness and the input–output kinematics of the silicon device, shown in Figs. 3(f) and 3(g). The force deflection of the devices is measured using a 20 g force sensor (FUTEK LSB200) with a resolution of 50 μN. The force transducer was mounted on a precision linear stage (PI Q-545), with a resolution of 1 nm and a minimum incremental motion

TABLE I. Design parameters for the monolithic frequency doubler transmission mechanism.

Parameters	a	L_{b_1}	L_{b_2}	L_1	L_2	L_3	H	h	φ
Values	4.3 mm	22.52 mm	13 mm	2.5 mm	3.5 mm	0.6 mm	1.8 mm	0.05 mm	37.5°

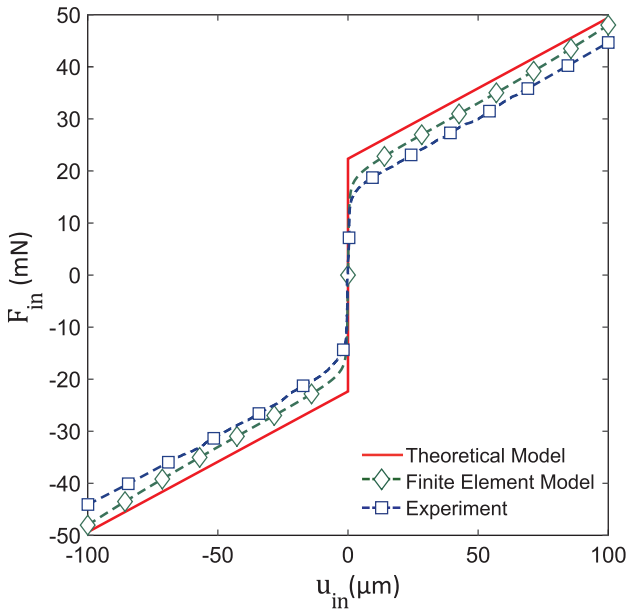

FIG. 4. Theoretical, experimental, and FEM results of the actuation force as the inputs displaced for $u_{in} = \pm 100\ \mu$m.

of 6 nm, to provide a rectilinear input motion. A displacement of $u_{in} = \pm 100\ \mu$m was applied to the input shuttle of the microdevice, while the movement of the output shuttle was simultaneously captured using an optical microscope. The output displacement was then analyzed using image processing, where the measurement was calibrated by the markers with a minimum feature size of 1.5 μm on the output shuttles, shown in Fig. 3(e). This resulted in a displacement measurement with an accuracy of 100 nm. The optical displacement measurement, the FEM, and the theoretical model show the same behavior and order of magnitude for the input–output kinematics. However, maximum discrepancies of 0.15% and 0.2% with the theoretical model were predicted and observed, for the input–output velocity ratio, by the FEM and the experiment, respectively, which can be explained by the accuracy of the theoretical model.

The results of force–displacement characteristics obtained by the experiment, the FEM, and the theoretical model are depicted in Fig. 4. A similar trend in actuation stiffness for both upward and downward input motion is observed. The results from FEM and experiment show a 21.2% and 30.4% decrease in buckling force predicted by the theoretical model, respectively. This can be explained by the accuracy of the classical Euler-Beam theory and the effect of the initial curvature of the beams, as a geometrical imperfection. Moreover, the discrepancy between the experimental results and the FEM can be explained by other imperfection factors and uncertainty in the thickness measurement, which is about $\pm 0.8\ \mu$m. A decrease in thickness t of 0.2 μm for buckle-sensitive beams with an initial average thickness of 21.5 μm results in an approximately 2.77% decrease in buckling force.

The modal frequencies of the proposed mechanism that alter its kinematics are calculated by FEM. The first undesired motion occurs at 650 Hz, corresponding to the out-of-plane movement. This is about two orders of magnitude higher than the operation frequency of the mechanism for application in mechanical watches, which is dictated by the natural frequency of the oscillator (about 5–15 Hz). Moreover, by further down scaling of the mechanism, using beams with a thickness of 2 μm, the application in devices within the frequency range of 10 kHz can be reached.

In summary, this paper proposes a monolithic micromechanical frequency doubler transmission mechanism. Frequency doubling functionality has been achieved by employing buckling of slender microflexures as reconfigurable kinematic joints and verified using both finite element analysis and experiments. Our future work includes concatenation of these frequency doubler building blocks for higher frequency advantages and characterization of their nonlinear dynamics experimentally.

This work was supported by TAG Heuer and LVMH Watches Division.

REFERENCES

[1]P. Ouyang, R. Tjiptoprodjo, W. Zhang, and G. Yang, "Micro-motion devices technology: The state of arts review," Int. J. Adv. Manuf. Technol. **38**, 463–478 (2008).
[2]K. R. Qalandar, B. Strachan, B. Gibson, M. Sharma, A. Ma, S. Shaw, and K. Turner, "Frequency division using a micromechanical resonance cascade," Appl. Phys. Lett. **105**, 244103 (2014).
[3]J. Wessels, D. F. Machekposhti, J. L. Herder, G. Sèmon, and N. Tolou, "Reciprocating geared mechanism with compliant suspension," J. Microelectromech. Syst. **26**, 1047–1054 (2017).
[4]D. F. Machekposhti, J. L. Herder, G. Sémon, and N. Tolou, "A compliant micro frequency quadrupler transmission utilizing singularity," J. Microelectromech. Syst. **27**, 506–512 (2018).
[5]B. S. Williams, "Terahertz quantum-cascade lasers," Nat. Photonics **1**, 517 (2007).
[6]Y. Yang, C. Callegari, X. Feng, K. Ekinci, and M. Roukes, "Zeptogram-scale nanomechanical mass sensing," Nano Lett. **6**, 583–586 (2006).
[7]F. Cottone, H. Vocca, and L. Gammaitoni, "Nonlinear energy harvesting," Phys. Rev. Lett. **102**, 080601 (2009).
[8]J. H. Lee, K. S. Hwang, D. S. Yoon, J. Y. Kang, S. K. Kim, and T. S. Kim, "Direct electrical measurement of protein–water interactions and temperature dependence using piezoelectric microcantilevers," Adv. Mater. **23**, 2920–2923 (2011).
[9]D. Yamane, T. Konishi, T. Matsushima, K. Machida, H. Toshiyoshi, and K. Masu, "Design of sub-1g microelectromechanical systems accelerometers," Appl. Phys. Lett. **104**, 074102 (2014).
[10]J. C. Long, H. W. Chan, A. B. Churnside, E. A. Gulbis, M. C. Varney, and J. C. Price, "Upper limits to submillimetre-range forces from extra space-time dimensions," Nature **421**, 922 (2003).
[11]R. G. Knobel and A. N. Cleland, "Nanometre-scale displacement sensing using a single electron transistor," Nature **424**, 291 (2003).
[12]Y. Wang and W. Zhang, "Stochastic vibration model of gear transmission systems considering speed-dependent random errors," Nonlinear Dyn. **17**, 187–203 (1998).
[13]G. Bonori and F. Pellicano, "Non-smooth dynamics of spur gears with manufacturing errors," J. Sound Vib. **306**, 271–283 (2007).
[14]Y. Guo and R. G. Parker, "Dynamic modeling and analysis of a spur planetary gear involving tooth wedging and bearing clearance nonlinearity," Eur. J. Mech.-A/Solids **29**, 1022–1033 (2010).
[15]L. L. Howell, *Compliant Mechanisms* (John Wiley and Sons, 2001).
[16]D. F. Machekposhti, N. Tolou, and J. Herder, "A statically balanced fully compliant power transmission mechanism between parallel rotational axes," Mech. Mach. Theory **119**, 51–60 (2018).
[17]S. Kota, J. Hetrick, Z. Li, and L. Saggere, "Tailoring unconventional actuators using compliant transmissions: Design methods and applications," IEEE/ASME Trans. Mechatron. **4**, 396–408 (1999).
[18]D. F. Machekposhti, N. Tolou, and J. Herder, "A fully compliant homokinetic coupling," J. Mech. Des. **140**, 012301 (2018).